Journal of Sound and Vibration (2002) **252**(3), 443–456
doi:10.1006/jsvi.2001.3849, available online at http://www.idealibrary.com on IDEAL®

LINEAR VIBRATION CHARACTERISTICS OF CABLE–BUOY SYSTEMS

W.-J. Kim and N. C. Perkins

Department of Mechanical Engineering, University of Michigan, 2250 G.G. Brown, Ann Arbor, MI 48109, U.S.A. E-mail: ncp@umich.edu

(*Received* 4 *October* 2000, *and in final form* 7 *June* 2001)

A theoretical model for the linear vibration of a cable tensioned by a subsurface buoy is developed. The equilibrium of the cable–buoy system subject to drag is evaluated using an approximate closed-form solution whose range of validity is confirmed through comparison with numerical solutions. The three-dimensional equations of cable–buoy motion are linearized about this equilibrium and then used to assess vibration characteristics. The characteristic equations for the natural frequencies of both in-plane and out-of-plane vibration modes are derived. The in-plane natural frequency spectrum exhibits the curve veering phenomena due to asymmetry of the associated mode shapes. Parameter studies reveal the dependencies of the in-plane and out-of-plane vibration modes on the cable tension, the buoy mass, and the current velocity.

1. INTRODUCTION

Cables are lightweight structural elements capable of transmitting forces and electrical and optical signals over great distances. Cables find pervasive use in ocean engineering applications where they serve as towing lines, mooring lines, signal transmission lines, umbilicals, tethers, etc. Growing interest in deep water resources requires the use of cable systems in, for example, mooring lines for floating production storage and offloading facilities, tension leg platforms, and remotely operated vehicles. The design of such systems benefits from accurate and efficient predictions of dynamic cable response due to environmental loading. This study focuses on the dynamic characteristics of an underwater cable attached to a subsurface buoy.

The ocean environment continuously disturbs a cable–buoy system through wave and current actions. For instance, a change in the mean current will alter the equilibrium position of the buoy and the equilibrium shape and tension of the cable. These changes in the equilibrium subsequently alter the vibration characteristics of the cable–buoy system.

The natural frequencies and mode shapes for shallow sagged cables with fixed and level supports have been studied extensively; see, for example, Irvine and Caughey [1] and reviews in references [2, 3]. The dynamic characteristics of shallow sag cables with fixed but inclined supports was considered in reference [2] by assuming a symmetrical equilibrium configuration (about the mid-span of the cable). This study concluded that the cable natural frequency spectrum possesses frequency cross overs as in the case of level supports. Triantafyllou and Grinfogel [4] accounted for the asymmetry of the equilibrium configuration for an inclined cable and concluded that the natural frequency spectrum

0022-460X/02/$35.00

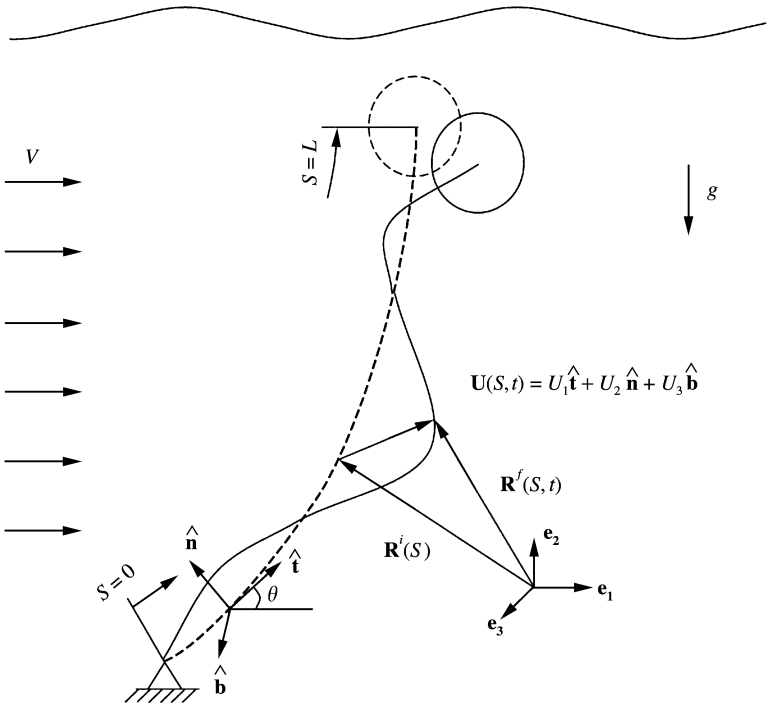

Figure 1. Schematic of cable with length L tensioned by a spherical buoy and subject to a uniform current. Three-dimensional dynamic response (—— curve) from equilibrium (– – – – curve) is described by $\mathbf{U}$ which is resolved into components along the Serret–Frenet triad $\{\hat{t}, \hat{n}, \hat{b}\}$ defined by the equilibrium configuration.

exhibits "avoided crossing" (also known as curve veering [5]) and asymmetric vibration mode shapes.

The cables used in mooring or towing applications are frequently assumed to be massless spring elements [6] or inertia-free inextensible segments [7]. In these instances, attention is focused on the moored or towed body assuming that the cable only provides a non-linear or linear restoring force. The introduction of cable inertia leads to partial differential equations for the cable coupled to the ordinary differential equations for the body; see, for example, references [8, 9].

The objective of this paper is to determine the linear vibration characteristics of cable–buoy systems composed on an inclined elastic cable fixed at its lower end and terminating at a submerged buoy at its upper end; refer to Figure 1. Parameter studies are performed to identify the major influences of the cable–buoy parameters on the natural frequency spectrum and the associated vibration mode shapes.

2. EQUATIONS OF MOTION

Figure 1 illustrates the cable–buoy system of interest. The flexible cable is fixed to the sea bed at its lower end and attached to a buoy at its upper end. The equations governing three-dimensional cable–buoy response are developed below.

The cable is considered to be a homogeneous, linearly elastic, one-dimensional continuum with negligible torsional, bending and shear rigidities, and subject to gravity, tension and fluid forces. The cable model follows that of cable-mass systems developed in

reference [10] with fluid forces considered in reference [11]. The fluid forces on the buoy and cable are approximated by using Morison's equation and do not include possible fluctuating lift and drag components due to vortex shedding. The equations of three-dimensional motion about an equilibrium configuration are derived as follows.

Figure 1 illustrates the cable in its equilibrium configuration (dashed curve) subject to a uniform current and in its dynamic (solid curve) configuration following a disturbance. The position vectors $\mathbf{R}^i(S)$ and $\mathbf{R}^f(S, t)$ describe the location of a material point on the cable centerline in the equilibrium and dynamic configurations respectively. The three-dimensional dynamic response of the cable about equilibrium $\mathbf{U}(S, t) = \mathbf{R}^f(S, t) - \mathbf{R}^i(S)$ is projected onto the equilibrium Serret–Frenet triad composed of the unit tangent ($\hat{\mathbf{t}}$), normal ($\hat{\mathbf{n}}$), and binormal ($\hat{\mathbf{b}}$) directions. Hence, $\mathbf{U}(S, t) = U_1(S, t)\hat{\mathbf{t}} + U_2(S, t)\hat{\mathbf{n}} + U_3(S, t)\hat{\mathbf{b}}$, where S denotes the equilibrium arc length co-ordinate and t denotes time. The co-ordinates U_1 and U_2 define responses within the equilibrium plane and U_3 defines response orthogonal to this plane.

Following references [10, 11], the kinetic and strain energies of the cable and buoy are formulated together with the virtual work done by gravitational and fluid forces. Substituting those expressions into Hamilton's principle leads to the following equations of motion for the cable–buoy system:

$$mU_{1,tt} = [\Psi]_{,S} - K^i\psi(U_{2,s} + K^iU_1) - m_eg\sin\theta + F_{DT}, \tag{1}$$

$$m'U_{2,tt} = [\psi(U_{2,S} + K^iU_1)]_{,S} + K^i\Psi - m_eg\cos\theta + F_{DN}, \tag{2}$$

$$m'U_{3,tt} = [\psi U_{3,S}]_{,S} + F_{DB} \tag{3}$$

with boundary conditions

$$\text{at } S = 0: \quad U_j(0, t) = 0, \quad j = 1, 2, 3, \tag{4}$$

$$\text{at } S = L: \quad M'\ddot{U}_1^L = (B - W)\sin\theta^L + H_1 - \Psi^L, \tag{5}$$

$$M'\ddot{U}_2^L = (B - W)\cos\theta^L + H_2 - \psi^L(U_{2,S}^L + K^LU_1^L), \tag{6}$$

$$M'\ddot{U}_3^L = H_3 - \psi^L(U_{3,S}^L). \tag{7}$$

The quantities $\Psi = \psi(1 + U_{1,S} - K^iU_2)$ and $\psi = P^i + EAh(S, t)$ describe the total tension of the cable. Here, EA denotes the axial stiffness of the cable cross-section and $h(S, t)$ denotes the dynamic strain of the cable centerline [10]. In the above equations, P^i and K^i are the equilibrium tension and curvature of the cable, respectively. The cable mass/length in air is $m = \rho_cA$, and that in water is $m' = (\rho_c + C_{ac}\rho_f)A$, where the fluid added mass (with added mass coefficient for the cable C_{ac}) is included. The effective cable weight/length is $m_eg = (\rho_c - \rho_f)Ag$ which includes the buoyancy of the cable. Here, ρ_c is the cable density, ρ_f is the fluid density, g is the acceleration due to gravity, and A is the (uniform) cable cross-sectional area. Note that the fluid added mass is small in tangential direction and therefore ignored in equation (1). The quantity θ is the angle of inclination of the equilibrium tangent from the horizontal as depicted in Figure 1.

Note that Archimedes' principle is not applicable to the infinitesimal cable element since the hydrostatic pressure field is not closed [12]. To account for this, the force due to hydrostatic pressure is added to the cross-sectional area of the cable element and then subtracted from the equilibrium tension. This modified tension, often called the "effective tension" [13], becomes

$$P^e = P^i + P_sA, \tag{8}$$

where P_s is the hydrostatic pressure at the location of the cable element. However, for a taut cable, the effective tension can be approximated as P^i recognizing that $P^i \gg P_s A$ in shallow to moderate water depths. This approximation is used herein.

In equations (1)–(3), F_{DT}, F_{DN}, and F_{DB} represent components of hydrodynamic drag in the tangential, normal, and binormal directions, respectively, as given by [14]

$$F_{DT} = \tfrac{1}{2}\rho_f C_{DT}\pi D(V_t - U_{1,t})|V_t - U_{1,t}|, \tag{9}$$

$$F_{DN} = \tfrac{1}{2}\rho_f C_{DN} D(V_n - U_{2,t})|V_n - U_{2,t}|, \tag{10}$$

$$F_{DB} = \tfrac{1}{2}\rho_f C_{DN} D(-U_{3,t})|-U_{3,t}|, \tag{11}$$

where $V_t = V\cos\theta$ and $V_n = -V\sin\theta$ are the tangential and normal components of the uniform current. Here, C_{DT} and C_{DN} are the tangential and normal drag coefficients for an inclined cylinder. Experimental observations on flow past inclined cylinders show that the streamlines in the neighborhood of the cylinder are bent so that the actual flow is nearly orthogonal to the cylinder when $\theta \geqslant 55^\circ$ [15]. Therefore, C_{DN} can be approximated as the drag coefficient C_D for flow normal to the cylinder. Also, experiments reveal that C_{DT} is less than C_{DN} by an order of magnitude (typically 1–3% of C_{DN}); hence, F_{DT} will be ignored relative to F_{DN} and F_{DB} in the following.

The equations of motion for the buoy are expressed by the boundary conditions (5)–(7). The buoy mass, including fluid added mass, is $M' = M + C_{aB}\rho_f V_B$, where M, C_{aB}, and V_B are the buoy mass in air, added mass coefficient, and volume, respectively. In equations (5) and (6), B and W denote the buoyancy and weight of the buoy, respectively, and the superscript $()^L$ denotes a quantity evaluated at $S = L$. The hydrodynamic drag on the buoy is given by [16]

$$H_1 = \tfrac{1}{2}\rho_f C_{DB} A_B(V_x)|V_x|\cos\theta^L, \tag{12}$$

$$H_2 = \tfrac{1}{2}\rho_f C_{DB} A_B(-V_x)|-V_x|\sin\theta^L, \tag{13}$$

$$H_3 = \tfrac{1}{2}\rho_f C_{DB} A_B(-U^L_{3,t})|-U^L_{3,t}|, \tag{14}$$

where $V_x = V - U^L_{1,t}\cos\theta^L + U^L_{2,t}\sin\theta^L$, and C_{DB} and A_B are the drag coefficient and the projected area of the (spherical) buoy to the flow, respectively. Note that the hydrodynamic drag for the buoy in the flow direction is decomposed into components along the tangential and normal directions since the independence principle of the drag coefficient for an infinite cylinder does not hold for finite three-dimensional bodies such as a spherical buoy.

3. EQUILIBRIUM ANALYSIS

Prior to evaluating the linear vibration characteristics of the cable–buoy system, the equilibrium tension $P^i(S)$ and the inclination angle $\theta^i(S)$ must first be determined. Using $U_1 \equiv U_2 \equiv U_3 \equiv 0$ in equations (1)–(3) yields the following equilibrium equations governing $P^i(S)$ and $K^i(S)$:

$$P^i_{,S} = m_e g\sin\theta^i, \qquad P^i K^i = m_e g\cos\theta^i - \tfrac{1}{2}\rho_f C_D D V^i_n|V^i_n|, \tag{15, 16}$$

where $V^i_n = -V\sin\theta^i$ and the superscript $()^i$ denotes a quantity evaluated in the equilibrium configuration. In arriving at equations (15) and (16), $F_{DT} \ll F_{DN}$, $C_{DN} \cong C_D$, and $K^i(S) = \theta^i_{,S}(S)$ were used. The above equations can be integrated numerically starting at $S = L$ where the equilibrium tension and angle are known for a specific buoy. While

analytical solutions to equations (15) and (16) are not available, approximate closed-form solutions can be obtained using the following approximations.

Consider a relatively taut inclined cable and expand $\theta^i(S)$ in a first order Taylor series about the point $S = l$, $0 \leqslant l \leqslant L$ where $\theta = \theta^*$:

$$\theta_a^i \cong \theta^* + R(S - l). \tag{17}$$

The slope R may be determined by knowing the angle at the upper end $\theta^L = \tan^{-1}((B - W)/H)$ and the lower end angle where (approximately) $\theta^0 \cong \tan^{-1}[((B - W) - m_e gL)/(H + \frac{1}{2}\rho_f C_D DLV^2)]$. Here, H is the magnitude of the hydrodynamic drag on buoy in the flow direction. Using equation (17), the fluid force components can now be evaluated and force balances on the cable element in the horizontal and vertical directions provide

$$\cos\theta^i(S) = \frac{1}{P^i}\left[H - \frac{1}{24R}\rho_f C_D DV^2(9C_1 - C_2)\right], \tag{18}$$

$$\sin\theta^i(S) = \frac{1}{P^i}\left[(B - W) - m_e g(L - S) - \frac{1}{24R}\rho_f C_D DV^2(3S_1 - S_2)\right], \tag{19}$$

from which

$$P^i(S) = \left\{[(B - W) - m_e g(L - S)]^2 + H^2 + \frac{m_e g}{12R}\rho_f C_D DV^2[3\sin\theta_a^L - \sin(3\theta_a^L)](L - S) + \frac{m_e g}{36R^2}\rho_f C_D DV^2(9C_1 - C_2)\right\}^{1/2}, \tag{20}$$

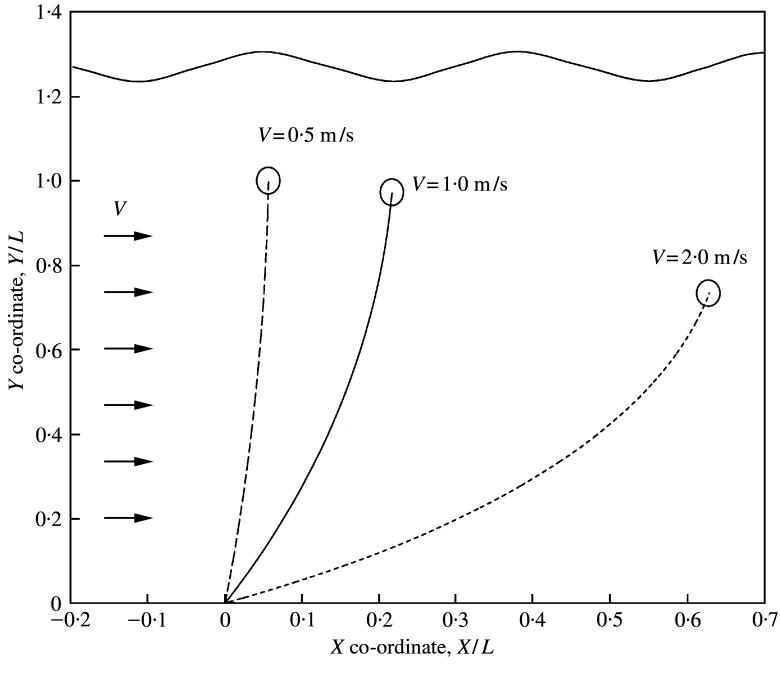

Figure 2. Equilibrium configuration of the example cable–buoy system defined in Table 1 at $V = 0{\cdot}5$ (– – – –), 1·0 (——), and 2·0 (· · ·) m/s. The net buoyancy of the buoy is five times the weight of the cable, i.e., $R_w = 5$.

TABLE 1

Cable, buoy and fluid parameters for examples in sections 3 *and* 5

Parameter	Value	Parameter	Value
Cable length (L)	40 m	Cable diameter (D)	0·0155 m
Cable density (ρ_c)	4104·52 kg/m^3	Fluid density (ρ_f)	1025 kg/m^3
Section modulus (EA)	$3{\cdot}1 \times 10^6$ N	Cable added mass coeff. (C_{ac})	1·0
Buoy added mass coeff. (C_{aB})	0·5	Cable drag coefficient (C_D)	1·05
Buoy drag coefficient (C_{DB})	0·4	Fluid velocity (V)	1 m/s

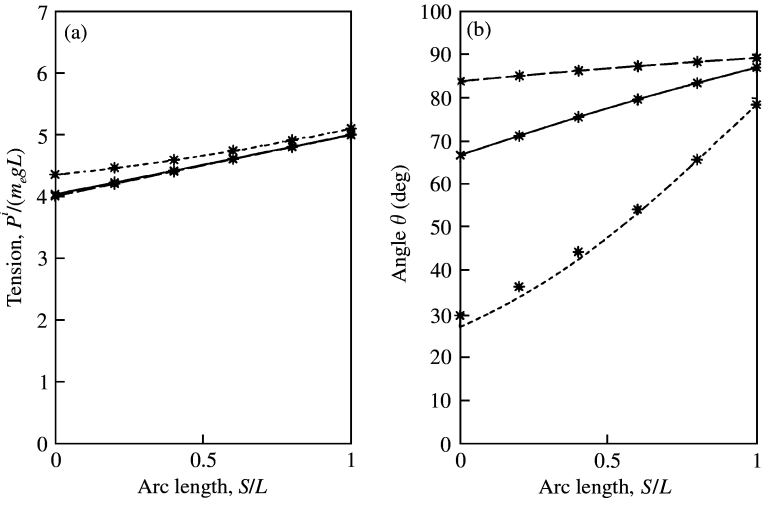

Figure 3. Predicted (a) equilibrium tension and (b) inclination angle at $V = 0{\cdot}5$ (– –), 1·0 (——), and 2·0 (· · · ·) m/s as a function of cable arc length when $R_w = 5$. Results of numerical integration are denoted by ****.

where $C_1 = \cos\theta_a^L - \cos\theta_a^i$, $C_2 = \cos(3\theta_a^L) - \cos(3\theta_a^i)$, $S_1 = \sin\theta_a^L - \sin\theta_a^i$, $S_2 = \sin(3\theta_a^L) - \sin(3\theta_a^i)$, and $\theta_a^L = \theta^* + R(L - l)$. The equilibrium curvature $K^i(S)$ can now be found by substituting equations (18)–(20) into equation (16) and solving for $\theta^i_{,S}$.

Figure 2 illustrates the equilibrium shape of a cable–buoy system defined by the example system parameters listed in Table 1. The cable–buoy system is illustrated for three values of the fluid velocity. The net buoyancy of the buoy ($B - W$) is 5 times the weight of the cable in this example leading to a relatively taut cable profile for all fluid velocities considered. The numerical solution of equations (15) and (16) confirms the accuracy of the approximate closed-form solution above whenever

$$R_w = (B - W)/(m_e gL) > 2. \tag{21}$$

For example, when this condition is met, the approximate solution is accurate to within 2% (0·4%) based upon the inclination angle $\theta^i(S)$ (the equilibrium tension $P^i(S)$) at any position along the cable for the nominal case $V = 1$ m/s. The corresponding equilibrium tension and inclination angle of the cable are illustrated in Figure 3 and exhibit good agreement with numerical results (asterisks). Note that the cable tension is dominated by the buoyancy of the buoy for the relatively taut cables considered herein. This fact is also reflected in the

computed inclination angle which varies almost linearly (i.e., almost constant, small curvature) along the cable.

4. EIGENSOLUTION ANALYSIS

The natural frequencies and mode shapes of the cable–buoy system play an important role in any subsequent analysis of dynamic response and particularly vortex-induced vibrations. These quantities may be determined upon linearizing the equations of motion about the equilibrium configuration. To this end, the equilibrium equations (15) and (16) are substituted into equations (1)–(7) and excitation, drag and non-linear terms are ignored. Furthermore, it is assumed that the equilibrium sag is small and that the cable stretches quasi-statically (ignore term $U_{1,tt}$ in equation (1)) since longitudinal waves in the cable propagate extremely fast relative to transverse waves [17]. However, the tangential acceleration of the buoy in equation (5) is retained to capture the relatively slow time scale dynamics of the buoy due to the (expected) large buoy inertia.

The equilibrium analysis above reveals that the equilibrium tension $P^i(S)$ and curvature $K^i(S)$ of a taut cable are nearly constant and shall be approximated as such hereafter†. Applying Taylor series expansions about $S = l = L$ in equation (17) and using $P^i \cong P^L$ and $K^i \cong K^L$, the equations of motion (1)–(7) linearized about the equilibrium configuration become

$$\frac{m'}{m_e} D u_{2,tt} = v_t^2 u_{2,ss} + v_l^2 k G(t), \qquad \frac{m'}{m_e} D u_{3,tt} = v_t^2 u_{3,ss} \tag{22, 23}$$

with boundary conditions

$$\text{at } s = 0: \quad u_j(s, t) = 0, \quad j = 2, 3, \tag{24}$$

$$\text{at } s = \frac{L}{D}: \quad \frac{M'}{m_e} \ddot{u}_2^L = -v_t^2 u_{2,s}^L, \quad \frac{M'}{m_e} \ddot{u}_3^L = -v_t^2 u_{3,s}^L, \tag{25, 26}$$

where

$$G(t) = \frac{D}{L}\left[u_1^L - \int_0^{L/D} k u_2 \, \mathrm{d}s \right] \tag{27}$$

is the dynamic strain of the cable centerline. The tangential displacement at the buoy u_1^L satisfies the equation of motion

$$\ddot{u}_1^L + \omega_1^2 u_1^L = \omega_1^2 \int_0^{L/D} k u_2 \, \mathrm{d}s. \tag{28}$$

Here, $\omega_1^2 = EA/(LM')$ is the natural frequency of cable–buoy system in the tangential direction and is the same as that of a massless elastic rod with stiffness EA/L and end mass M'. The following non-dimensional quantities are employed in equations (22)–(28):

$$s = \frac{S}{D}, \quad k = K^L D, \quad u_j = \frac{U_j}{D}, \quad j = 1, 2, 3,$$

$$\frac{v_t^2}{g} = \frac{P^L}{m_e D g} \quad \text{and} \quad \frac{v_l^2}{g} = \frac{EA}{m_e D g}.$$

†One can also relax this assumption and allow first order variation in the tension and curvature as in reference [4].

The associated eigenvalue problems are found by substituting

$$u_1^L(t) = X_1 e^{i\omega_2 t}, \quad u_2(s,t) = X_2(s)e^{i\omega_2 t}, \quad u_3(s,t) = X_3(s)e^{i\omega_3 t} \tag{29}$$

into equations (22)–(28), where ω_2 and ω_3 represent the natural frequencies for vibration modes within the plane of the equilibrium and normal to the plane of the equilibrium, respectively. The mode shapes for these "in-plane" and "out-of-plane" modes are given by $X_2(S)$ and $X_3(S)$ respectively.

The characteristic equation for the natural frequencies of the in-plane modes is found as

$$\left[-\lambda^2 - \left(z_1\lambda^2 + \frac{v_l^2}{v_t^2}\right)\eta_2^2 + z_1\eta_2^4\right]\sin(\eta_2) + 2z_1\lambda^2\eta_2 + \left[-\eta_2^3 + \left(\frac{v_l^2}{z_1 v_t^2} + \lambda^2 - 2z_1\lambda^2\right)\eta_2\right]\cos(\eta_2) = 0, \tag{30}$$

where $z_1 = M'/(m'L)$ denotes the mass ratio of the buoy to the cable and $\lambda^2 = (v_l kL)^2/(v_t^2 D^2)$ represents a cable parameter for an inclined cable [2]. The eigenvalue $\eta_2 = L\phi_2/D$ in equation (30) is found numerically where $\phi_2^2 = m'D\omega_2^2/(m_e v_t^2)$. The corresponding in-plane mode shape is

$$X_2(s) = \cos(\phi_2 s) + \frac{[z_1\eta_2\tan(\eta_2/2) - 1]\tan(\eta_2)}{[z_1\eta_2\tan(\eta_2) - 1]}\sin(\phi_2 s) - 1. \tag{31}$$

The characteristic equation for the natural frequencies of the out-of-plane modes is

$$\cos(\eta_3) = z_1\eta_3\sin(\eta_3) \tag{32}$$

and the corresponding out-of-plane mode shape is

$$X_3(s) = \sin(\phi_3 s), \tag{33}$$

where the eigenvalue $\eta_3 = L\phi_3/D$ can be found numerically and $\phi_3^2 = m'D\omega_3^2/(m_e v_t^2)$.

5. RESULTS

The parameters for the examples used in this study are listed in Table 1. Consider first two simple limiting cases obtained when the buoy mass approaches zero and then infinity. As the buoy mass approaches zero, $z_1 \to 0$, the characteristic equations and associated natural frequencies for the in-plane ($j = 2$) and out-of-plane ($j = 3$) modes become

$$\cos(\eta_j) = 0, \quad \omega_j = \left(\frac{2n-1}{2}\right)\frac{\pi}{L}\sqrt{\frac{P^L}{m'}}, \quad n = 1, 2, \ldots. \tag{34}$$

Thus, the classical results for a taut string with one end fixed and one end free are recovered as required in this limit (assuming non-vanishing tension). The computed natural frequencies for this limiting case are illustrated in Figure 4(a) for the in-plane modes and the left limits of Figure 5 for the out-of-plane modes. Both in-plane and out-of-plane natural frequencies are trivial functions of the cable parameter λ/π as $z_1 \to 0$. In these and subsequent figures, the natural frequencies are represented as non-dimensional quantities and are normalized by the fundamental natural frequency of a taut string with fixed supports, ω_s. The corresponding mode shapes are illustrated in Figures 6–8 where they are

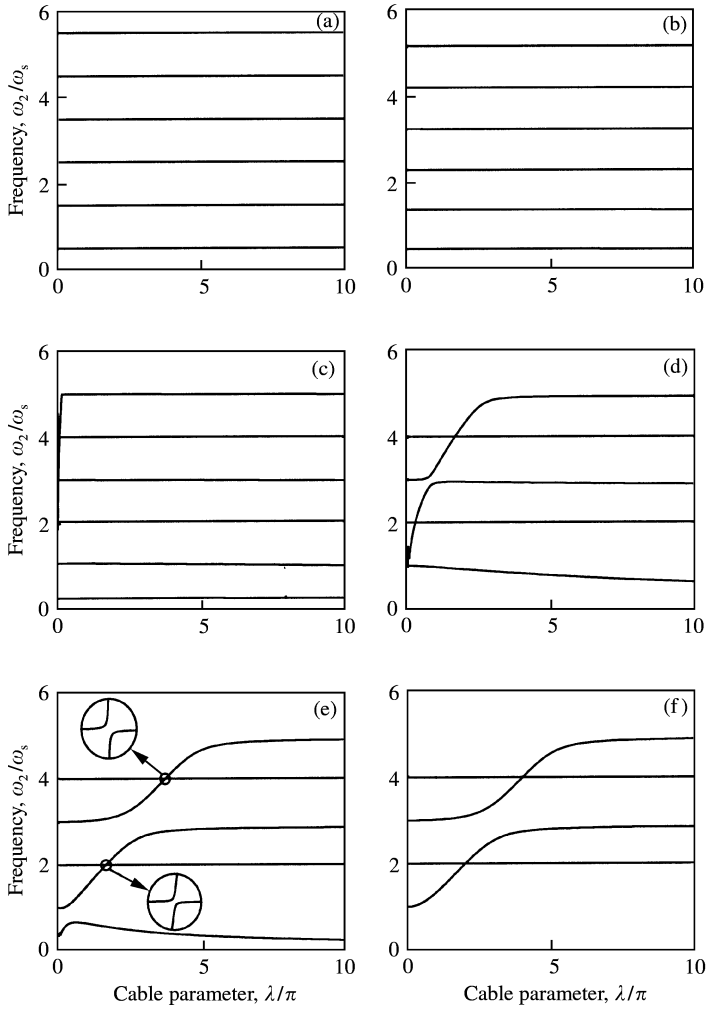

Figure 4. In-plane natural frequency spectra as functions of the cable parameter λ/π for six values of the buoy mass: (a) $z_1 \to 0$, (b) $z_1 = 0{\cdot}1$, (c) $z_1 = 1$, (d) $z_1 = 10$, (e) $z_1 = 100$, and (f) $z_1 \to \infty$. Natural frequencies are normalized with respect to the fundamental natural frequency of a string with fixed supports (ω_s).

denoted by the value $z_1 = 0$. In this limit, there is no (first order) dynamic stretching of the cable centerline as there is no resistance at the boundary $S = L$.

For the limiting case of infinite buoy mass, $z_1 \to \infty$, we recover the case of an inclined cable with fixed supports. The characteristic equation (30) provides

$$\eta_2 - \frac{\eta_2^3}{\lambda^2} = 2\tan\left(\frac{\eta_2}{2}\right) \tag{35}$$

for symmetric in-plane modes which have frequency cross-overs at $\lambda/\pi = 2n$, $n = 1, 2, 3, \ldots$ [2]. The natural frequencies of the antisymmetric in-plane modes and all of the out-of-plane modes are identical to those of the classical taut string with fixed supports. The in-plane natural frequencies are illustrated in Figure 4(f) as a function of the cable parameter λ/π. The out-of-plane natural frequencies are illustrated in the right limits of Figure 5 and are

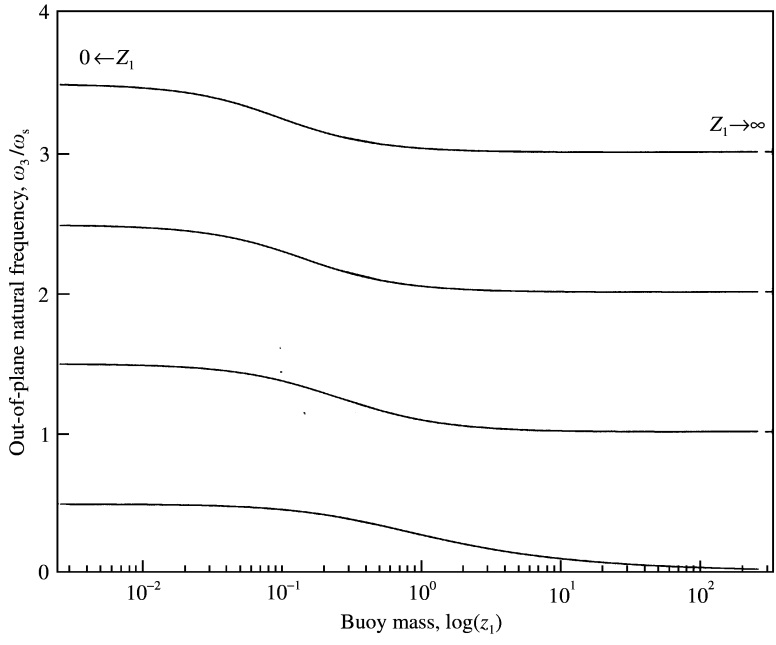

Figure 5. Out-of-plane natural frequency spectrum as a function of buoy mass z_1 for buoy diameter $d = 0{\cdot}6$ m and cable parameter $\lambda/\pi = 6$. Natural frequencies are normalized with respect to the fundamental natural frequency of a string with fixed supports (ω_s).

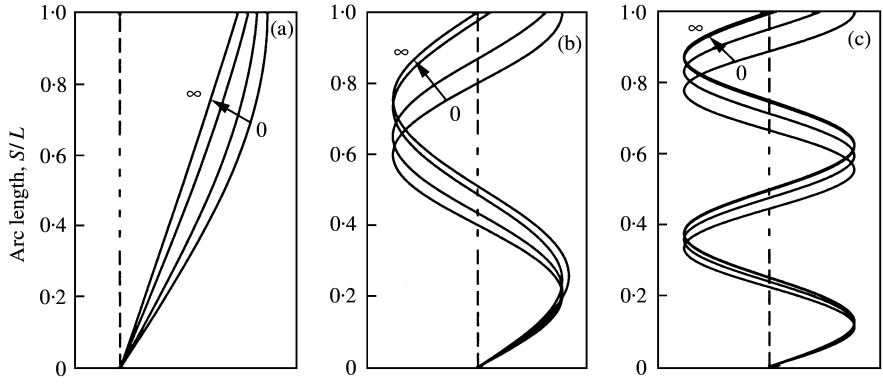

Figure 6. Odd-order in-plane mode shapes for selected values of the buoy mass for the case $\lambda/\pi = 10$. Buoy mass $z_1 = 0$, 0·1, 1, and ∞. (a) first mode, (b) third mode, and (c) fifth mode. – – – line represents the equilibrium configuration of the cable.

independent of the cable parameter. The corresponding mode shapes are illustrated in Figures 6–8 where they are denoted by the value $z_1 \rightarrow \infty$. It should be restated that these results are based on assuming an equilibrium shape that is symmetric about the cable mid-span (as in reference [2]). If the equilibrium is allowed to be asymmetric (as in reference [4]), the in-plane natural frequency spectrum, Figure 4(f), would exhibit curve veering instead of crossings and hybrid (asymmetric) mode shapes would exist.

Consider now the general case of finite (and non-vanishing) buoy mass. Figure 4 shows the in-plane natural frequency spectrum parameterized by the buoy mass. Note that the

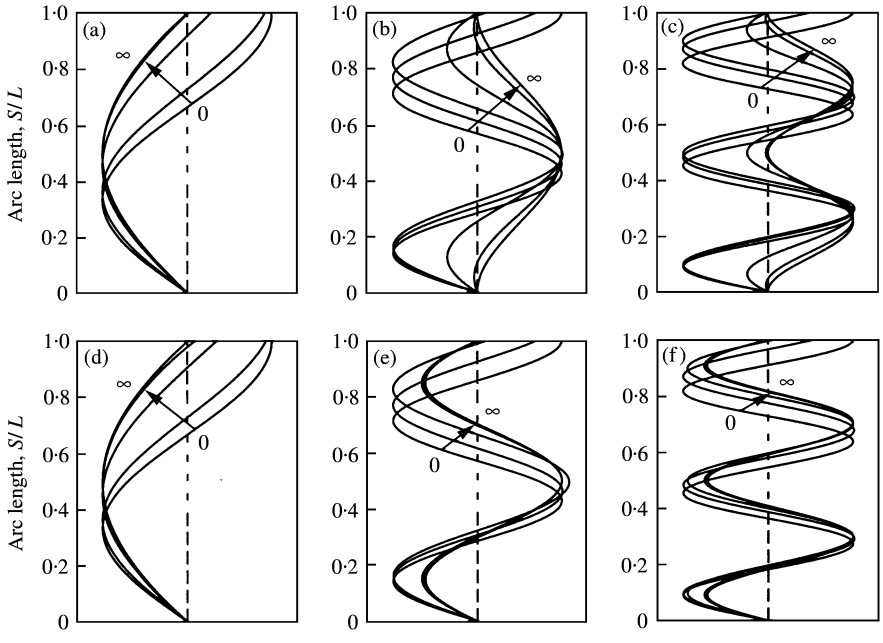

Figure 7. Even-order in-plane mode shape for selected values of the cable parameter λ/π and buoy mass z_1. Buoy mass $z_1 = 0$, 0·1, 1, 30, 100, and ∞. (a) and (d) second mode at $\lambda/\pi = 0{\cdot}8$ and 10, (b) and (e) fourth mode at $\lambda/\pi = 2$ and 10, and (c) and (f) sixth mode at $\lambda/\pi = 4$ and 10. – – – line represents the equilibrium configuration of the cable.

fourth and sixth natural frequencies for vanishing buoy mass ($z_1 \to 0$) evolve to the natural frequencies of the first and second symmetric modes, respectively, as the buoy mass approaches infinity ($z_1 \to \infty$) and the third and fifth natural frequencies evolve to the first and second antisymmetric modes as the buoy mass increases from 0 to ∞. Note also from Figure 4(e) that the natural frequencies never exhibit cross-overs (repeated frequencies). Instead curve veering occurs when the buoy mass is finite. Curve veering originates from the asymmetry of the mode shapes as discussed in reference [4]. Moreover, as the buoy mass increases, the location of the veering regions migrate from $\lambda/\pi = 0$ for vanishing buoy mass ($z_1 \to 0$) to $\lambda/\pi = 2n$, $n = 1, 2, \ldots$ for infinite buoy mass ($z_1 \to \infty$). Therefore, the vibration characteristics of cable–buoy systems become more sensitive to parameter changes for cases of moderate cable tension. Finally, the natural frequencies are strongly sensitive to changes in the cable parameter whenever the vibration mode shape includes significant dynamic stretching.

The corresponding mode shapes are illustrated in Figure 6 (odd order modes) and Figure 7 (even order modes) for selected values of the buoy mass. Note that as the buoy mass increases, the first and second natural frequencies approach zero and the first mode approximates a pendulum-like mode (no nodes) as shown in Figure 6(a). The fourth and higher order even in-plane mode shapes become sensitive to the cable parameter λ/π as the buoy mass increases ($z_1 \to \infty$). For example, the fourth in-plane mode shape evolves from the first symmetric mode for fixed supports at $\lambda/\pi = 2$ in Figure 7(b) to the second symmetric mode at $\lambda/\pi = 10$ as illustrated in Figure 7(e). The first symmetric in-plane mode shape for fixed supports continuously evolves to the second symmetric mode and thereby minimizes the dynamic cable tension.

The out-of-plane natural frequency spectrum is illustrated in Figure 5 as a function of the buoy mass when $\lambda/\pi = 6$. Unlike the in-plane natural frequencies, the out-of-plane natural

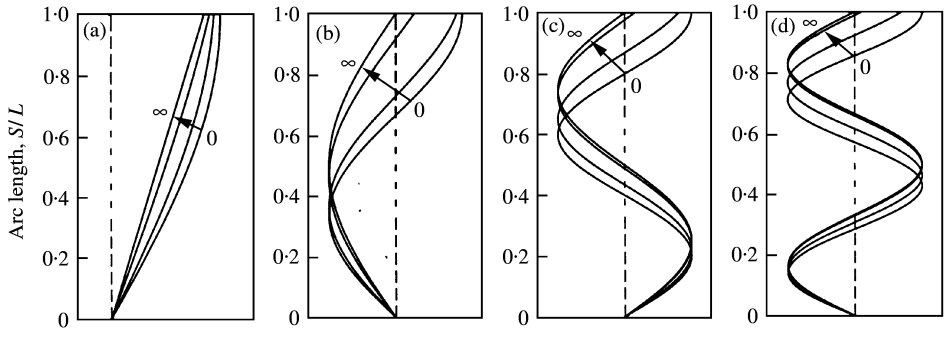

Figure 8. Out-of-plane mode shape for selected values of the buoy mass: $z_1 = 0, 0{\cdot}1, 1,$ and ∞. (a) first mode, (b) second mode, (c) third mode, and (d) fourth mode. – – – line represents the equilibrium configuration of the cable.

frequencies are independent of the cable parameter λ/π since they do not induce dynamic stretching. The fundamental natural frequency for vanishing buoy mass ($z_1 \to 0$) approaches zero with increasing buoy mass and the corresponding mode shape approaches a pendulum-like mode as expected; see Figure 8(a). The second and third natural frequencies evolve to the first and second out-of-plane natural frequencies of an inclined cable with fixed supports, respectively. The out-of-plane natural frequency spectrum shows rapid changes at moderate buoy mass ($0{\cdot}1 < z_1 < 1$) and also shows earlier transitions from those of fixed–free supports to fixed supports at higher vibration modes.

Figure 9 shows the in-plane natural frequency spectrum as a function of the flow velocity for six values of the buoy mass. The flow velocity controls the hydrodynamic drag which then controls the equilibrium curvature and tension, hence the natural frequencies. Note that the accuracy of the approximate equilibrium solution initially degrades with an increase in the flow velocity because the linear inclination angle approximation in equation (17) initially deviates from the exact solution. However, increasing flow velocity also creates more drag on the buoy and eventually more tension. These effects make the uniform curvature and tension accurate in the range of moderate flow velocity (0–4 m/s). In this range, the first in-plane natural frequency approaches zero with increasing buoy mass and it is not sensitive to the flow velocity. However, the second natural frequency significantly depends on the flow velocity and the buoy mass. With increasing flow velocity, the equilibrium curvature of the cable first increases and then decreases towards zero. The second natural frequency achieves its minimum value when the curvature achieves its maximum ($V \cong 3.75$ m/s) since the cable becomes structurally softer with greater curvature. The natural frequencies of the third and higher order, odd in-plane modes are nearly independent of the flow velocity for moderate buoy mass ($z_1 = 0{\cdot}1, 1, 10$). With increasing buoy mass, however, frequency veerings appear; refer to "v's" denoted in Figure 9. The natural frequencies exhibit considerable dependence on the flow velocity for the case of higher buoy mass ($z_1 \geqslant 20$) and the sensitivity is greatest within the range of flow velocities expected in the ocean environment (0–2 m/s).

6. SUMMARY AND CONCLUSION

A model for the linear vibration characteristics of cable–buoy systems subject to a uniform current has been developed. The equilibrium of the cable–buoy system is evaluated first and the associated equilibrium tension and curvature are determined from

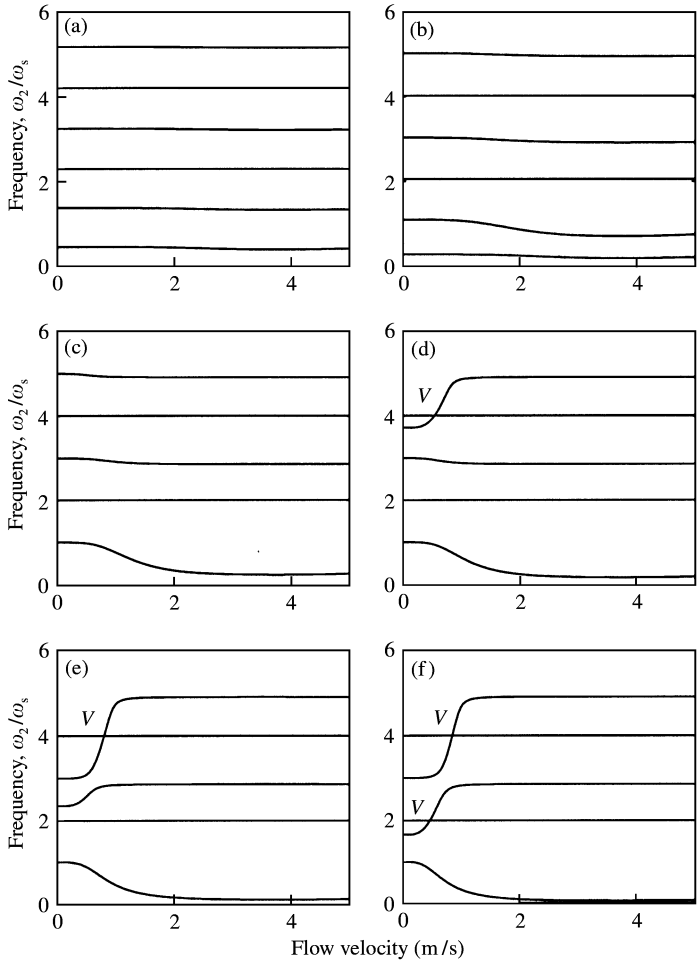

Figure 9. In-plane natural frequencies as functions of the flow velocity for buoy diameter $d = 0{\cdot}6\ m$ and $R_w = 5$. (a) $z_1 = 0{\cdot}1$, (b) $z_1 = 1$, (c) $z_1 = 10$, (d) $z_1 = 20$, (e) $z_1 = 50$, and (f) $z_1 = 100$. Natural frequencies are normalized with respect to the fundamental natural frequency of a string with fixed supports (ω_s). In the figure, 'V' denotes a region of curve veering.

an approximate closed-form solution. The accuracy of this approximation is confirmed by comparison with results found by numerical integration.

The natural frequencies and mode shapes for the in-plane and out-of-plane modes of the cable–buoy system are studied. When the buoy mass approaches zero, the results converge to the classical cases of a taut string with fixed–free boundary conditions as required. At the other extreme, when the buoy mass approaches infinity, the results converge to those of a taut inclined cable with fixed supports. For finite and non-zero buoy mass, the natural frequencies and mode shapes are evaluated as functions of the cable parameter λ/π, buoy mass z_1, and flow velocity V. For the in-plane natural frequencies, frequency curve veering exists.

As the buoy mass increases, the first and second in-plane natural frequencies and the first out-of-plane natural frequency all converge to zero when the current exists. For both types of modes, the corresponding fundamental mode shape evolves to a pendulum-like mode for large buoy mass. The natural frequency spectrum for the in-plane modes exhibits a strong dependence on the cable parameter and flow velocity for cases of large buoy mass.

ACKNOWLEDGMENT

The authors wish to acknowledge the U.S. Office of Naval Research for support of this research.

REFERENCES

1. H. M. IRVINE and T. K. CAUGHEY 1974 *Proceedings of the Royal Society of London A* **341**, 299–315. The linear theory of free vibrations of a suspended cable.
2. H. M. IRVINE 1981 *Cable Structures*. Cambridge, MA: MIT Press.
3. M. S. TRIANTAFYLLOU 1984 *Shock and Vibration Digest* **16**, 9–17. Linear dynamics of cables and chains.
4. M. S. TRIANTAFYLLOU and L. GRINFOGEL 1986 *American Society of Civil Engineers Journal of Structural Engineering* **112**, 139–148. Natural frequencies and modes of inclined cables.
5. N. C. PERKINS and C. D. MOTE 1986 *Journal of Sound and Vibration* **106**, 451–463. Comments on curve veering in eigenvalue problems.
6. O. GOTTLIEB 1997 *American Society of Mechanical Engineers Journal of Offshore Mechanics and Arctic Engineering* **119**, 234–238. Bifurcations of a nonlinear small-body ocean-mooring system excited by finite-amplitude waves.
7. J. V. SANDERS 1982 *Ocean Engineering* **9**, 483–499. A three-dimensional dynamic analysis of a towed system.
8. A. A. TJAVARAS, Q. ZHU, Y. LIU, M. S. TRIANTAFYLLOU and D. K. P. YUE 1998 *Journal of Sound and Vibration* **213**, 709–737. The mechanics of highly-extensible cables.
9. J. M. ABEL 1972 *Journal of Hydronautics* **6**, 83–89. Cable interactions in a depth controlled submersible.
10. H. P. LIN and N. C. PERKINS 1995 *Journal of Sound and Vibration* **179**, 131–149. Free vibration of complex cable/mass systems: theory and experiment.
11. W.-J. KIM and N. C. PERKINS 2000 *Proceedings of ETCE/OMAE* 2000 *Joint Conference, New Orleans*, February 14–17, OMAE2000-8010. Nonlinear two dimensional vortex induced vibration of an elastic cable.
12. C. P. SPARKS 1984 *American Society of Mechanical Engineers Journal of Energy Resources Technology* **106**, 46–54. The influence of tension, pressure and weight on pipe and riser deformations and stresses.
13. M. S. TRIANTAFYLLOU and A. BLIEK 1983 *Proceedings* 15 *Annual Offshore Technology Conference*, **1**, 469–476. The dynamics of inclined taut and slack marine cables.
14. H. O. BERTEAUX 1976 *Buoy Engineering*, New York: John Wiley & Sons.
15. B. M. SUMER and J. FREDSOE 1999 *Hydrodynamics Around Cylindrical Structures*. New Jersey: World Scientific Publishing Co.
16. S. K. CHAKRABARTI 1987 *Hydrodynamics of Offshore Structures*. Boston: Computational Mechanics Publications.
17. M. BEHBAHANI-NEJAD and N. C. PERKINS 1996 *Journal of Sound and Vibration* **196**, 189–202. Freely propagating waves in elastic cables.